

Atmospheric Chemistry of HFC-272ca: Spectrokinetic Investigation of the CH₃CF₂CH₂O₂ Radical, Its Reactions with NO and NO₂, and the Fate of the CH₃CF₂CH₂O Radical

Trine E. Møgelberg, Ole J. Nielsen,* and Jens Sehested

Section for Chemical Reactivity, Environmental Science and Technology Department, Risø National Laboratory, DK-4000 Roskilde, Denmark

Timothy J. Wallington* and Michael D. Hurley

Ford Research Laboratory, SRL-3083, Ford Motor Company, P.O. Box 2053, Dearborn, Michigan 48121-2053

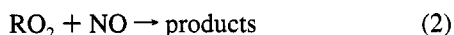
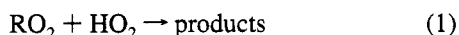
Received: September 20, 1994; In Final Form: November 17, 1994[⊗]

A pulse radiolysis technique has been used to investigate the UV absorption spectrum of the CH₃CF₂CH₂O₂ radical from HFC-272ca, CH₃CF₂CH₃. The absorption cross sections were quantified in the wavelength range 220–320 nm; at 250 nm the absorption cross section for CH₃CF₂CH₂O₂ was $\sigma = (451 \pm 59) \times 10^{-20} \text{ cm}^2 \text{ molecule}^{-1}$. By following the increase in NO₂ at 400 nm, the rate constant for the reaction of CH₃CF₂CH₂O₂ with NO was determined to be $(8.5 \pm 1.9) \times 10^{-12} \text{ cm}^3 \text{ molecule}^{-1} \text{ s}^{-1}$. The reaction of CH₃CF₂CH₂O₂ with NO₂ was found to have a reaction rate constant of $(6.8 \pm 0.5) \times 10^{-12} \text{ cm}^3 \text{ molecule}^{-1} \text{ s}^{-1}$. The kinetics of the reaction of CH₃CF₂CH₃ with F atoms and CH₃CF₂CH₂ with O₂ were studied. The rate constants were $(2.8 \pm 0.9) \times 10^{-11}$ and $(1.10 \pm 0.03) \times 10^{-12} \text{ cm}^3 \text{ molecule}^{-1} \text{ s}^{-1}$, respectively. The observed rate constant for the self-reaction of CH₃CF₂CH₂O₂ radicals was $(8.6 \pm 0.4) \times 10^{-12} \text{ cm}^3 \text{ molecule}^{-1} \text{ s}^{-1}$. The reaction of CH₃CF₂CH₂O₂ radicals with NO gives CH₃CF₂CH₂O radicals; the dominant atmospheric fate of CH₃CF₂CH₂O radicals is reaction with O₂ to give CH₃CF₂CHO. As part of the present work, relative rate techniques were used to measure rate constants at 296 ± 2 K for the reactions of Cl and F atoms with CH₃CF₂CH₃, with the values being $(1.7 \pm 0.2) \times 10^{-14}$ and $(3.3 \pm 0.8) \times 10^{-11} \text{ cm}^3 \text{ molecule}^{-1} \text{ s}^{-1}$, respectively.

Introduction

An international research effort is being carried out to investigate the environmental impact of the release of HFCs in the atmosphere. The study reported here is a continuation of previous work performed in our laboratory regarding the degradation of HFCs in the atmosphere.^{1,2}

The major loss process for HFCs in the atmosphere is reaction with OH radicals, resulting in the generation of halogenated alkyl radicals, which then rapidly react with O₂ to form peroxy radicals, RO₂. In the atmosphere RO₂ radicals react with HO₂, NO, NO₂, or other peroxy radicals R'O₂:³



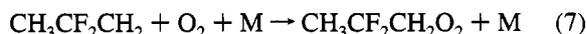
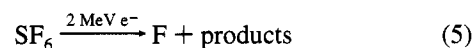
In this work we have studied reactions 2, 3, and 4 for the peroxy radical generated from HFC-272ca, CH₃CF₂CH₂O₂, which is presently under consideration as a CFC replacement.

Experimental Section

The two different experimental systems used in the present work have been described in detail previously^{4–6} and will only be discussed briefly here.

Pulse Radiolysis System. Radicals were generated by the irradiation of SF₆/O₂/HFC-272ca mixtures in a 1 L stainless steel reaction cell with a 30 ns pulse of 2 MeV electrons from

a Febetron 705B field emission accelerator. SF₆ was always in great excess and was used to generate fluorine atoms:



Transient absorptions were followed by multipassing the output of a pulsed 150 W xenon arc lamp through the reaction cell using internal White cell optics. Total path lengths of 80 and 120 cm were used. After exiting the cell the light was guided through a 1 m McPherson grating UV–vis monochromator and detected with a Hamamatsu photomultiplier. The spectral resolution was 0.8 nm. Reagent concentrations used were: SF₆, 900–950 mbar; O₂, 5–40 mbar; CH₃CF₂CH₃, 10–40 mbar; NO, 0.25–1.6 mbar; and NO₂, 0.40–1.25 mbar. All experiments were performed at 296 K. Ultrahigh purity O₂ was supplied by L'Air Liquide, SF₆ (99.9%) was supplied by Gerling and Holz, CH₃CF₂CH₃ (>97%) was obtained from PCR Inc., NO (99.8%) was obtained from Messer Grieshem, and NO₂ (>98%) was obtained from Linde Technische Gase. All reagents were used as received. The partial pressures of the different gases were measured with a Baratron absolute membrane manometer with a detection limit of 10⁻⁵ bar.

The following experiments were performed using the pulse radiolysis system. First, the ultraviolet absorption spectrum of CH₃CF₂CH₂O₂ radicals was determined by observing the maximum in the transient UV absorption at short times (0–5 μs). Second, the kinetics of the reaction of HFC-272ca with F atoms was studied by observing the maximum in the absorbance following the radiolysis of SF₆/O₂/CH₃CF₂CH₃ mixtures and

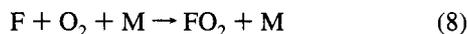
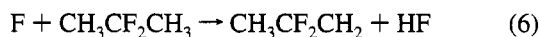
[⊗] Abstract published in *Advance ACS Abstracts*, January 1, 1995.

varying the $\text{CH}_3\text{CF}_2\text{CH}_3$ concentration. Third, the decay of $\text{CH}_3\text{CF}_2\text{CH}_2\text{O}_2$ was followed at long times up to $1000 \mu\text{s}$ to derive a value for the self-reaction rate constant. Fourth, the reaction of $\text{CH}_3\text{CF}_2\text{CH}_2$ radicals with O_2 was studied by observing the appearance of $\text{CH}_3\text{CF}_2\text{CH}_2\text{O}_2$ with various O_2 concentrations. Fifth, the kinetics of the reaction with NO_2 was determined by observing the decay in NO_2 concentration at 400 nm following the radiolysis of $\text{SF}_6/\text{O}_2/\text{CH}_3\text{CF}_2\text{CH}_3/\text{NO}_2$ mixtures. For the reaction with NO similar experiments were performed by varying the NO concentration and observing the increase in NO_2 concentration.

FTIR—Smog Chamber System. The FTIR system was interfaced to a 140 L Pyrex reactor as described previously.⁶ Radicals were generated by the UV irradiation of mixtures of 98–100 mTorr of $\text{CH}_3\text{CF}_2\text{CH}_3$, 0.4–0.5 Torr of F_2 , 5–147 Torr of O_2 in 700 Torr total pressure with N_2 diluent at 296 K using 22 black lamps (760 Torr = 1013 mbar). The loss of reactants and the formation of products were monitored by FTIR spectroscopy, using an analyzing path-length of 27 m and a resolution of 0.25 cm^{-1} . Infrared spectra were derived from 32 coadded spectra. $\text{CH}_3\text{CF}_2\text{CH}_3$ and COF_2 were monitored using their characteristic features over the wavenumber ranges 750–1450 and 700–800 cm^{-1} , respectively. Reference spectra were acquired by expanding known volumes of reference materials into the reactor. An authentic sample of $\text{CH}_3\text{CF}_2\text{CHO}$ was not available. The approach used to quantify the yield of $\text{CH}_3\text{CF}_2\text{CHO}$ was to compare the integrated absorption of the product feature in the region 1725–1800 cm^{-1} (the carbonyl stretching feature) with a calibrated reference spectrum of the structurally similar molecule CF_3CHO . Substitution of a F atom in CF_3CHO by a CH_3 group is not expected to have a substantial impact on the integrated absorption of the 1775 cm^{-1} feature.

Results and Discussion

Reaction of F + $\text{CH}_3\text{CF}_2\text{CH}_3$. The competition between reactions 6 and 8 was used to determine the rate for reaction 6:



The kinetics of reaction 6 was studied by performing a set of experiments where the concentration of O_2 was held fixed at 40 mbar, SF_6 was fixed at 960 mbar, and the $\text{CH}_3\text{CF}_2\text{CH}_3$ concentration was varied between 0 and 6 mbar.

Figure 1 shows the observed variation of the maximum absorbance at 250 nm as a function of the concentration ratio $[\text{CH}_3\text{CF}_2\text{CH}_3]/[\text{O}_2]$. Since at 250 nm the absorbance of $\text{CH}_3\text{CF}_2\text{CH}_2\text{O}_2$ is greater than that of an equal amount of FO_2 , the absorbance of the system increases with increasing $[\text{CH}_3\text{CF}_2\text{CH}_3]/[\text{O}_2]$ as $\text{CH}_3\text{CF}_2\text{CH}_2\text{O}_2$ replaces FO_2 . As shown in Figure 1, A_{max} increases until the $[\text{CH}_3\text{CF}_2\text{CH}_3]/[\text{O}_2]$ ratio is about 0.04. Further increase in the $[\text{CH}_3\text{CF}_2\text{CH}_3]/[\text{O}_2]$ ratio does not affect the maximum absorbance.

The solid line in Figure 1 represents a three-parameter fit of the following expression to the data:

$$A_{\text{max}} = \{A_{\text{FO}_2} + A_{\text{CH}_3\text{CF}_2\text{CH}_2\text{O}_2}(k_6/k_8)[\text{CH}_3\text{CF}_2\text{CH}_3]/[\text{O}_2]\} / \{1 + (k_6/k_8)[\text{CH}_3\text{CF}_2\text{CH}_3]/[\text{O}_2]\}$$

where A_{max} is the observed maximum absorbance, A_{FO_2} is the maximum absorbance expected if only FO_2 were produced, and $A_{\text{CH}_3\text{CF}_2\text{CH}_2\text{O}_2}$ is the maximum absorbance expected if $\text{CH}_3\text{CF}_2\text{CH}_2\text{O}_2$ were the sole absorbing species. Parameters A_{FO_2} ,

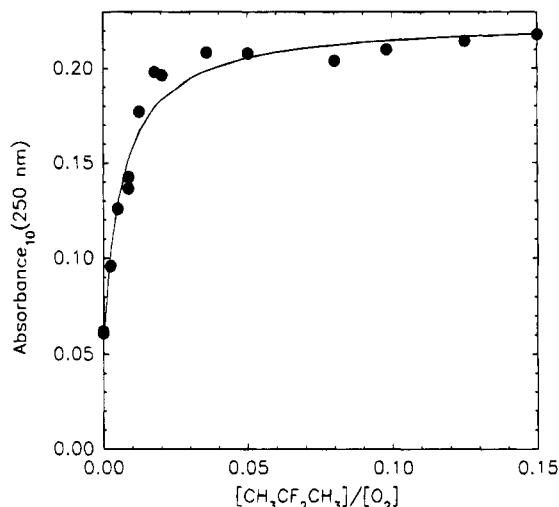


Figure 1. Plot of the maximum absorbance as a function of the concentration ratio $[\text{CH}_3\text{CF}_2\text{CH}_3]/[\text{O}_2]$.

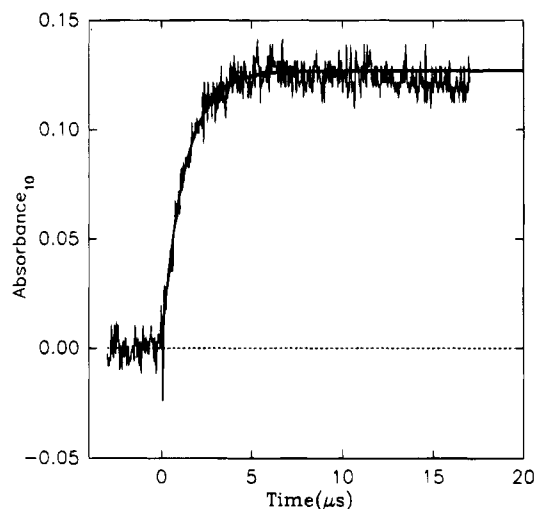


Figure 2. Absorption at 230 nm following the pulsed radiolysis of a mixture of 40 mbar of O_2 , 20 mbar of $\text{CH}_3\text{CF}_2\text{CH}_3$, and 940 mbar of SF_6 : single pulse, quarter dose, no signal averaging. The smooth line represents a first-order fit to the data and gives $k^{\text{1st}} = 8.5 \times 10^5 \text{ s}^{-1}$.

$A_{\text{CH}_3\text{CF}_2\text{CH}_2\text{O}_2}$, and k_6/k_8 were simultaneously varied. The best fit was obtained with $k_6/k_8 = (148 \pm 48)$. Using $k_8 = 1.9 \times 10^{-13} \text{ cm}^3 \text{ molecule}^{-1} \text{ s}^{-1}$ gives $k_6 = (2.8 \pm 0.9) \times 10^{-11} \text{ cm}^3 \text{ molecule}^{-1} \text{ s}^{-1}$.

$\text{CH}_3\text{CF}_2\text{CH}_2 + \text{O}_2$. To measure the kinetics of reaction 7, a series of experiments were performed where the $\text{CH}_3\text{CF}_2\text{CH}_3$ concentration was held constant at 20 mbar, the SF_6 concentration was held at 940 mbar, and the O_2 concentration varied between 20 and 60 mbar. Figure 2 shows a transient following radiolysis in the presence of 40 mbar of O_2 . The figure shows a fast increase in the absorbance which is complete after approximately $5 \mu\text{s}$. The rise in absorbance was fitted using a first-order expression. In the presence of 20 mbar of $\text{CH}_3\text{CF}_2\text{CH}_3$ the lifetime of F atoms is $< 0.1 \mu\text{s}$. To allow for sufficient time for conversion of F atoms into $\text{CH}_3\text{CF}_2\text{CH}_2$ radicals, the fit was started at $1 \mu\text{s}$. The pseudo-first-order rate constants were plotted as a function of O_2 concentration, and a linear least squares fit was performed. The result can be seen in Figure 3 and gives $k_7 = (1.10 \pm 0.03) \times 10^{-12} \text{ cm}^3 \text{ molecule}^{-1} \text{ s}^{-1}$.

UV Absorption Spectrum of $\text{CH}_3\text{CF}_2\text{CH}_2\text{O}_2$. Following the pulse radiolysis of a mixture of 40 mbar of O_2 , 20 mbar of $\text{CH}_3\text{CF}_2\text{CH}_3$, and 940 mbar of SF_6 , a rapid increase (complete within $5 \mu\text{s}$) in the UV absorption was observed. It seems

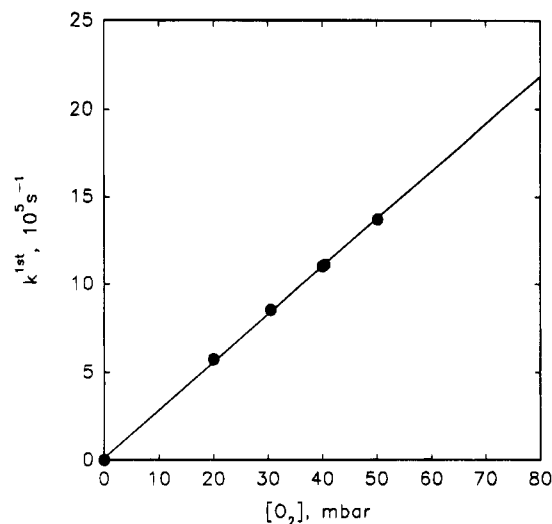
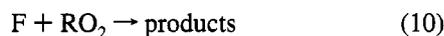


Figure 3. k^{1st} versus $[O_2]$.

reasonable to ascribe this absorbance to the formation of the $CH_3CF_2CH_2O_2$ radical. Before we are able to calculate the absorption cross sections we need to know the F atom yield and to consider possible complications. The F atom yield at full dose was measured recently in our laboratory, and the value obtained was $(2.83 \pm 0.30) \times 10^{15} \text{ cm}^{-3}$ at full radiation dose and 1000 mbar of SF_6 . The method involves measuring the absorbance at 260 nm due to CH_3O_2 following pulse radiolysis of $CH_4/O_2/SF_6$ and is described in detail elsewhere.⁷ Also we need to consider secondary chemistry. After the electron pulse, reactions 6 and 8 compete for the available F atoms. In our experiments we used 40 mbar of O_2 and 20 mbar of $CH_3CF_2CH_3$. With these concentrations and the rate constants $k_6 = 2.8 \times 10^{-11} \text{ cm}^3 \text{ molecule}^{-1} \text{ s}^{-1}$ and $k_8 = 1.9 \times 10^{-13} \text{ cm}^3 \text{ molecule}^{-1} \text{ s}^{-1}$,⁸ it can be calculated that 1.3% of the F atoms are converted into FO_2 . Finally we have to consider unwanted radical-radical reactions such as



To check for these reactions a set of experiments were performed with mixtures of 40 mbar of O_2 , 20 mbar of $CH_3CF_2CH_3$, and 940 mbar of SF_6 varying the radiolysis dose over 1 order of magnitude and plotting the maximum absorbance at 250 nm as a function of radiolysis dose. The UV path length was 80 cm. The result can be seen in Figure 4. The maximum absorbance was linear with the dose up to about 40% of the maximum dose. At higher dose the absorbance was smaller than expected from a linear extrapolation of the points at lower dose. We ascribe the curvature to incomplete conversion of F atoms to $CH_3CF_2CH_2O_2$ caused by secondary radical-radical reactions.

The solid line drawn through the data in Figure 4 is a linear least squares fit of the low-dose data. The slope is 0.42 ± 0.01 . From this value and three additional pieces of information, (i) the yield of F atoms of $(2.83 \pm 0.30) \times 10^{15} \text{ molecules cm}^{-3}$ (full dose and $[SF_6] = 1000 \text{ mbar}$), (ii) the conversion of F atoms into 98.7% $CH_3CF_2CH_2O_2$ and 1.3% FO_2 , (iii) the absorption cross section for FO_2 at 250 nm, $\sigma = 130 \times 10^{-20} \text{ cm}^2 \text{ molecule}^{-1}$,⁸ we derive $\sigma(CH_3CF_2CH_2O_2)$ at 250 nm = $(451 \pm 59) \times 10^{-20} \text{ cm}^2 \text{ molecule}^{-1}$. The quoted error includes both statistical and potential systematic errors and so reflects the accuracy of the measurement.

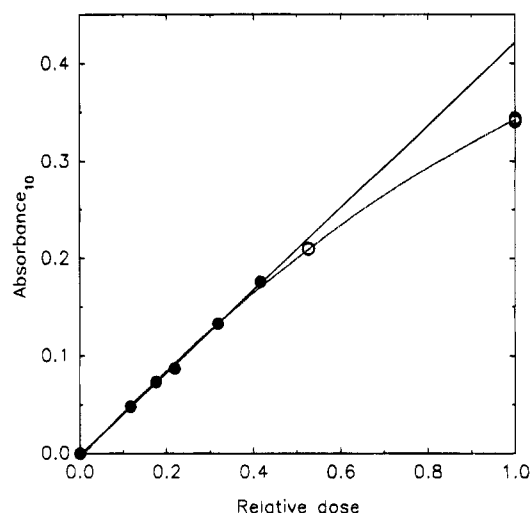


Figure 4. Maximum transient absorbance as a function of radiolysis dose at 250 nm following the pulsed radiolysis of 20 mbar of $CH_3CF_2CH_3$, 40 mbar of O_2 , and 940 mbar of SF_6 .

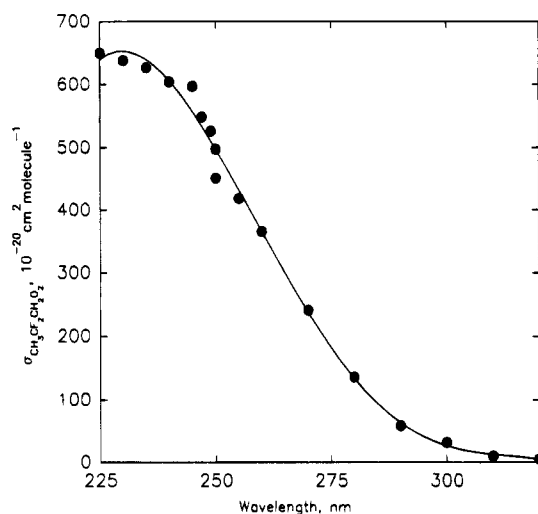


Figure 5. Absorption cross sections for $CH_3CF_2CH_2O_2$. The solid line is a fifth-order polynomial fit to help visual inspection.

TABLE 1: Measured UV Absorption Cross Sections

wavelength (nm)	$\sigma \times 10^{20}$ ($\text{cm}^2 \text{ molecule}^{-1}$)	wavelength (nm)	$\sigma \times 10^{20}$ ($\text{cm}^2 \text{ molecule}^{-1}$)
220	594	255	418
225	650	260	365
230	638	270	241
235	627	280	137
240	604	290	59
245	597	300	32
247	549	310	10
249	498	320	5
250	451		

To map out the spectrum of the $CH_3CF_2CH_2O_2$ radical, experiments were performed to measure the maximum transient absorbance between 220 and 320 nm following the pulsed irradiation of $SF_6/CH_3CF_2CH_3/O_2$ mixtures. The observed absorbance values were scaled to that at 250 nm and corrected for FO_2 to obtain absolute absorption cross sections. Absorption cross sections are given in Table 1 and shown in Figure 5.

Kinetic Data for the $CH_3CF_2CH_2O_2$ Self-Reaction. After the rapid increase in UV absorbance in the region 220–320 nm following the pulsed radiolysis of mixtures of 20 mbar of $CH_3CF_2CH_3$, 40 mbar of O_2 , and 940 mbar of SF_6 a slower decay was observed. We ascribe the decay in absorbance to the self-reaction of the $CH_3CF_2CH_2O_2$ radical.



The observed self-reaction rate constant for reaction 12 is defined as $-\text{d}[\text{CH}_3\text{CF}_2\text{CH}_2\text{O}_2]/\text{d}t = 2k_{12\text{obs}}[\text{CH}_3\text{CF}_2\text{CH}_2\text{O}_2]^2$. Figure 6 shows the reciprocal half-life for the decay of the absorption at 250 nm as a function of the initial absorbance due to $\text{CH}_3\text{CF}_2\text{CH}_2\text{O}_2$ radicals. The absorbance is corrected for the absorption of FO_2 . A linear least squares fit of the corrected data in Figure 6 gives a slope of $(0.733 \pm 0.002) \times 10^5 \text{ s}^{-1} = (k_{12\text{obs}} \times 2 \ln(10))/(\sigma(\text{CH}_3\text{CF}_2\text{CH}_2\text{O}_2) \times 120 \text{ cm})$. The intercept of the linear regression of the data is not significantly different from zero. Using $\sigma(\text{CF}_3\text{CF}_2\text{CH}_2\text{O}_2) = 451 \times 10^{-20} \text{ cm}^2 \text{ molecule}^{-1}$ at 250 nm, $k_{12\text{obs}} = (8.6 \pm 0.4) \times 10^{-12} \text{ cm}^3 \text{ molecule}^{-1} \text{ s}^{-1}$ was derived. $k_{12\text{obs}}$ may be an overestimate of the true bimolecular rate constant for reaction 12, as the $\text{CH}_3\text{CF}_2\text{CH}_2\text{O}_2$ radical might react with the reaction products, as discussed in ref 9.

The Kinetics of the Reaction $\text{CH}_3\text{CF}_2\text{CH}_2\text{O}_2 + \text{NO}$. The kinetics of reaction 2 was studied by monitoring the increase in absorbance at 400 nm following the radiolysis of mixtures of $\text{CH}_3\text{CF}_2\text{CH}_3/\text{O}_2/\text{SF}_6/\text{NO}$. NO_2 absorbs at 400 nm, and it is reasonable to ascribe the absorbance to NO_2 formation via reaction 2. This method of measuring the reaction of peroxy radicals with NO has been used extensively in our laboratory and has been discussed in detail elsewhere.^{10,11} The traces were fitted using first-order kinetics, and the resulting pseudo-first-order rate constants, k^{1st} were plotted as a function of NO concentration. As seen from Figure 7, the pseudo-first-order rate constant, k^{1st} , increased linearly with $[\text{NO}]$. Linear least squares analysis gives $k_2 = (7.71 \pm 0.71) \times 10^{-12} \text{ cm}^3 \text{ molecule}^{-1} \text{ s}^{-1}$. The y-axis intercept in Figure 7 is $(0.45 \pm 0.14) \times 10^5 \text{ s}^{-1}$. The cause of this intercept may be a small contribution to the $\text{CH}_3\text{CF}_2\text{CH}_2\text{O}_2$ decay caused by the self-reaction of $\text{CH}_3\text{CF}_2\text{CH}_2\text{O}_2$ radicals.

To assess the impact of the $\text{CH}_3\text{CF}_2\text{CH}_2\text{O}_2$ self-reaction on the measured value of k_2 , the formation of NO_2 was modeled using the CHEMSIMUL chemical kinetic modeling package¹² with a mechanism consisting of reactions 2, 3, 6, 7, 8, and 13 with $k_2 = 1 \times 10^{-11}$, $k_3 = 6 \times 10^{-12}$, $k_6 = 2.8 \times 10^{-11}$, $k_7 = 1.1 \times 10^{-12}$, $k_8 = 1.9 \times 10^{-13}$, $k_{12} = 8.6 \times 10^{-12}$, and $k_{13} = 3.0 \times 10^{-11} \text{ cm}^3 \text{ molecule}^{-1} \text{ s}^{-1}$:



In addition, reactions of NO with $\text{CH}_3\text{CF}_2\text{CH}_2$ and $\text{CH}_3\text{CF}_2\text{CH}_2\text{O}$ radicals were included assuming $k_{\text{CH}_3\text{CF}_2\text{CH}_2+\text{NO}}$ and $k_{\text{CH}_3\text{CF}_2\text{CH}_2\text{O}+\text{NO}} = 1 \times 10^{-11} \text{ cm}^3 \text{ molecule}^{-1} \text{ s}^{-1}$. A first-order fit was made to the simulated NO_2 results. In all cases the simulated data were well fit by first-order kinetics. The pseudo-first-order rates of NO_2 formation were slightly higher than the expected values given by $k_2[\text{NO}]$ with the difference increasing with decreasing $[\text{NO}]$. Corrections for the effect of the self-reaction on our measured kinetics for NO_2 formation were computed by detailed modeling of each data point. Corrected data are shown in Figure 7. Linear least squares analysis of the corrected data gives $k_2 = (8.49 \pm 0.70) \times 10^{-12} \text{ cm}^3 \text{ molecule}^{-1} \text{ s}^{-1}$ with a y-axis intercept of $(0.19 \pm 0.14) \times 10^5 \text{ s}^{-1}$. The cause of this small intercept is unknown. We estimate that potential systematic errors could add an additional 20% to the uncertainty range of k_2 . Propagating this additional 20% uncertainty gives $k_2 = (8.5 \pm 1.9) \times 10^{-12} \text{ cm}^3 \text{ molecule}^{-1} \text{ s}^{-1}$. This value is slightly smaller than the values of the rate constants $k_{\text{CFH}_2\text{O}_2+\text{NO}} = (12.5 \pm 1.3) \times 10^{-12} \text{ cm}^3 \text{ molecule}^{-1} \text{ s}^{-1}$ ¹¹ and $k_{\text{CF}_3\text{CH}_2\text{O}_2+\text{NO}} = (12 \pm 3) \times 10^{-12} \text{ cm}^3 \text{ molecule}^{-1} \text{ s}^{-1}$.² This may be due to steric effects as discussed by Sehested et al.¹¹

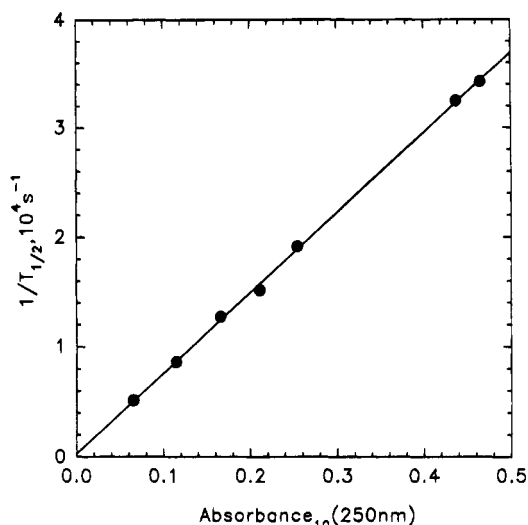


Figure 6. Plot of $1/T_{1/2}$ as a function of A_{max} at 250 nm.

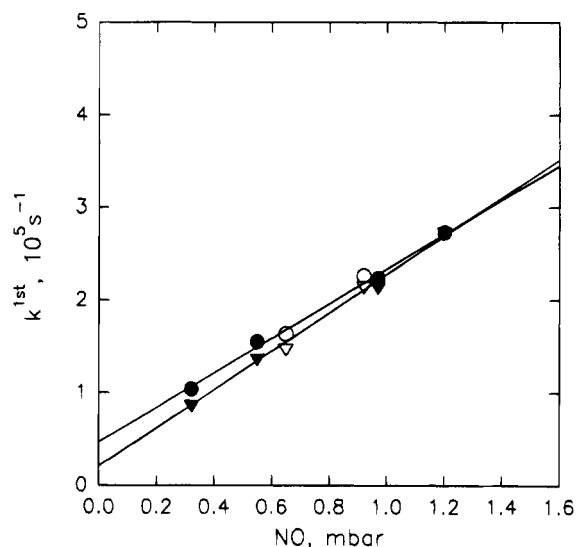


Figure 7. Plot of k^{1st} versus $[\text{NO}]$. Filled circles correspond to points taken at 400 nm, hollow circles at 450 nm. The triangles correspond to data that have been corrected for the effect of the $\text{CH}_3\text{CF}_2\text{CH}_2\text{O}_2$ self-reaction; see text for details.

The increase in absorbance at 400 nm can be combined with the literature value of $\sigma_{(\text{NO}_2)}(400 \text{ nm}) = 6.0 \times 10^{-19} \text{ cm}^2 \text{ molecule}^{-1}$ ¹⁷ to calculate the yield of NO_2 in this system. The yield of NO_2 in the four experiments given in Figure 7, expressed as moles of NO_2 produced per mole of F atoms consumed, was $63 \pm 9\%$. In the calculation, corrections were made for the loss of F atoms, via reaction 8 using $k_8 = 1.9 \times 10^{-13} \text{ cm}^3 \text{ molecule}^{-1} \text{ s}^{-1}$ and via reaction with NO producing FNO , using $k_{\text{F}+\text{NO}\rightarrow\text{FNO}} = 5.1 \times 10^{-12} \text{ cm}^3 \text{ molecule}^{-1} \text{ s}^{-1}$ (average from refs 13 and 14). The absorption of FNO at 400 nm is negligible. The fact that the yield of NO_2 is less than 100% is not unexpected. The self-reaction of $\text{CH}_3\text{CF}_2\text{CH}_2\text{O}_2$ radicals is sufficiently rapid that a significant fraction of the $\text{CH}_3\text{CF}_2\text{CH}_2\text{O}_2$ radicals undergo self-reaction. Using the chemical mechanism discussed above and assuming that reaction 2 gives exclusively NO_2 , then the NO_2 yield, calculated using the CHEMSIMUL modeling package,¹² varies from 74% to 75% as the NO is varied from 0.32 to 0.97 mbar.

While the results from the present work do not preclude the possibility of the presence of a minor channel leading to products other than NO_2 , it is clear that the majority of the reactions of $\text{CH}_3\text{CF}_2\text{CH}_2\text{O}_2$ radicals with NO give NO_2 and (by inference) $\text{CH}_3\text{CF}_2\text{CH}_2\text{O}$ radicals.

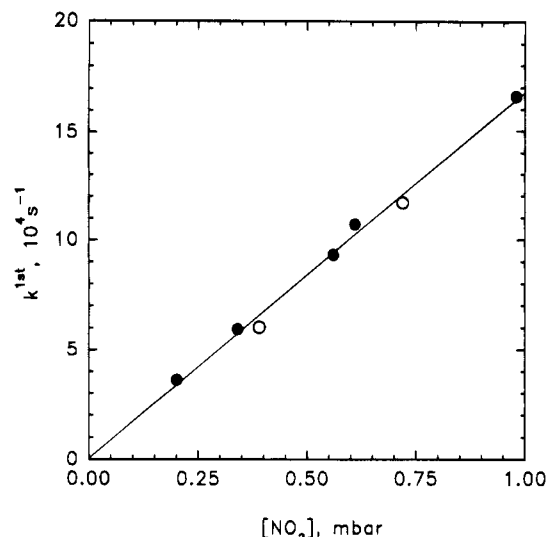


Figure 8. Plot of k^{1st} versus $[\text{NO}_2]$. Filled circles correspond to points taken at 400 nm, hollow circles at 450 nm.

The Reaction of $\text{CH}_3\text{CF}_2\text{CH}_2\text{O}_2$ with NO_2 . The kinetics of reaction 3 was studied by monitoring the absorbance at 400 nm following the radiolysis of mixtures of 20 mbar of $\text{CH}_3\text{CF}_2\text{CH}_3$, 40 mbar of O_2 , 0.3–0.97 mbar of NO_2 , and SF_6 to 1000 mbar total pressure. A number of experiments with varying NO_2 concentrations were performed, and the results are plotted in Figure 8. Linear least squares analysis of the data in Figure 8 gives $k_3 = (6.8 \pm 0.5) \times 10^{-12} \text{ cm}^3 \text{ molecule}^{-1} \text{ s}^{-1}$. There is a potential complication associated with the reaction of F atoms with NO_2 in reaction 13. Under the experimental conditions with a maximum pressure of 0.97 mbar of NO_2 used and $k_{13} = 3.0 \times 10^{-11} \text{ cm}^3 \text{ molecules}^{-1} \text{ s}^{-1}$,¹³ it can be calculated that only 5% of the F atoms react with NO_2 . Reaction 13 is not a significant complication under these experimental conditions. Our measured value for the reaction of $\text{CH}_3\text{CF}_2\text{CH}_2\text{O}_2$ with NO_2 is consistent with the high-pressure-limit values in the range $(4.5\text{--}8.9) \times 10^{-12} \text{ cm}^3 \text{ molecule}^{-1} \text{ s}^{-1}$ reported by Lightfoot et al.¹⁵ for the reaction of halogenated peroxy radicals with NO_2 .

Relative Rate Studies of the Reactions of Cl and F Atoms with $\text{CH}_3\text{CF}_2\text{CH}_3$. Prior to investigating the atmospheric fate of $\text{CH}_3\text{CF}_2\text{CH}_2\text{O}$ radicals, a series of relative rate experiments were performed using the FTIR system to investigate the kinetics of reactions 6 and 15. The techniques used are described in detail elsewhere.¹⁶ Photolysis of molecular halogen was used as a source of halogen atoms.



The kinetics of reaction 15 was measured relative to (16) and (17); reaction 6 was measured relative to (18) and (19).



The observed losses of $\text{CH}_3\text{CF}_2\text{CH}_3$ versus CH_4 and CD_4 in the presence of either Cl or F atoms are shown in Figures 9

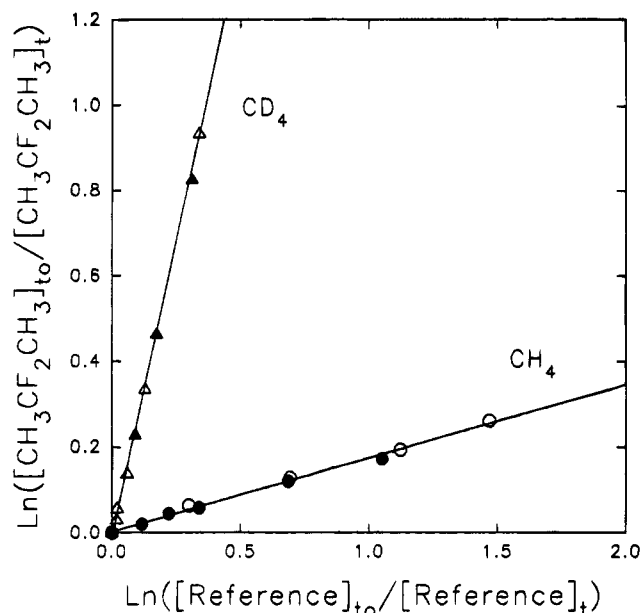


Figure 9. Plot of the decay of $\text{CH}_3\text{CF}_2\text{CH}_3$ versus those of CH_4 and CD_4 in 700 Torr of air (filled symbols) or nitrogen (open symbols) at 296 K in the presence of Cl atoms.

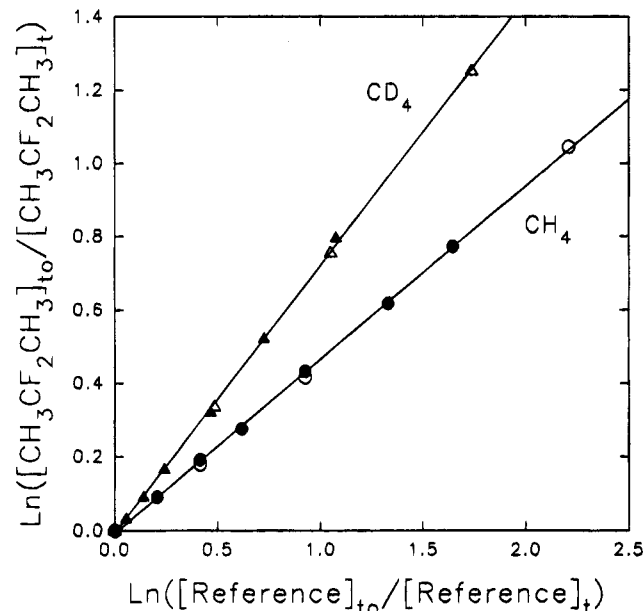
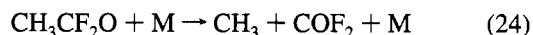
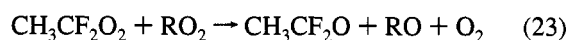
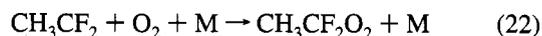
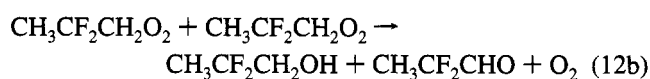
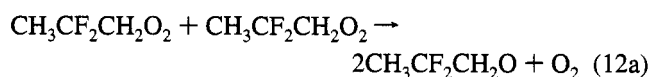


Figure 10. Plot of the decay of $\text{CH}_3\text{CF}_2\text{CH}_3$ versus those of CH_4 and CD_4 in 700 Torr of air (filled symbols) or nitrogen (open symbols) at 296 K in the presence of F atoms.

and 10, respectively. As shown in Figures 9 and 10, there was no discernible difference between data obtained in 700 Torr of either N_2 or air diluent. Linear least squares analysis gives $k_{15}/k_{16} = 0.17 \pm 0.01$, $k_{15}/k_{17} = 2.77 \pm 0.12$, $k_6/k_{18} = 0.47 \pm 0.02$, and $k_6/k_{19} = 0.73 \pm 0.03$. Using $k_{16} = 1.0 \times 10^{-13}$,¹⁷ $k_{17} = 6.1 \times 10^{-15}$,¹⁶ $k_{18} = 6.8 \times 10^{-11}$,¹⁸ and $k_{19} = 4.7 \times 10^{-11}$ ¹⁸ gives $k_{15} = (1.7 \pm 0.1) \times 10^{-14}$, $k_{15} = (1.7 \pm 0.1) \times 10^{-14}$, $k_6 = (3.2 \pm 0.2) \times 10^{-11}$, and $k_6 = (3.4 \pm 0.2) \times 10^{-11} \text{ cm}^3 \text{ molecule}^{-1} \text{ s}^{-1}$, respectively. We estimate that potential systematic errors associated with uncertainties in the reference rate constant could add an additional 10% and 20% to the uncertainty ranges for k_{15} and k_6 , respectively. Propagating this additional uncertainty gives values of $k_{15} = (1.7 \pm 0.2) \times 10^{-14}$, $k_{15} = (1.7 \pm 0.2) \times 10^{-14}$, $k_6 = (3.2 \pm 0.7) \times 10^{-11}$, and $k_6 = (3.4 \pm 0.7) \times 10^{-11} \text{ cm}^3 \text{ molecule}^{-1} \text{ s}^{-1}$. We choose to cite final values of k_{15} and k_6 which are averages of those determined

using the two different reference compounds together with error limits which encompass the extremes of the two individual determinations. Hence, $k_{15} = (1.7 \pm 0.2) \times 10^{-14}$ and $k_6 = (3.3 \pm 0.8) \times 10^{-11} \text{ cm}^3 \text{ molecule}^{-1} \text{ s}^{-1}$. Quoted errors reflect the accuracy of our measurements. The value of k_6 determined using the FTIR technique is in agreement with the determination of $k_6 = (2.8 \pm 0.9) \times 10^{-11} \text{ cm}^3 \text{ molecule}^{-1} \text{ s}^{-1}$ using the pulse radiolysis technique in the present work. There are no literature data for k_{15} or k_6 with which to compare our results.

Atmospheric Fate of $\text{CH}_3\text{CF}_2\text{CH}_2\text{O}$ Radicals. To determine the atmospheric fate of the alkoxy radical $\text{CH}_3\text{CF}_2\text{CH}_2\text{O}$, experiments were performed in which $\text{F}_2/\text{CH}_3\text{CF}_2\text{CH}_3/\text{O}_2$ mixtures at a total pressure of 700 Torr made up with N_2 diluent were irradiated in the FTIR-smog chamber system. The loss of $\text{CH}_3\text{CF}_2\text{CH}_3$ and the formation of products were monitored by FTIR spectroscopy. $\text{CH}_3\text{CF}_2\text{CH}_2\text{O}$ radicals formed in the chamber in reaction 12 will either react with O_2 to give the aldehyde $\text{CH}_3\text{CF}_2\text{CHO}$ or dissociate to give CH_3CF_2 radicals, which will be converted by reactions 22–24 into COF_2 .



By monitoring the formation of $\text{CH}_3\text{CF}_2\text{CHO}$ and COF_2 , the relative importance of reactions 20 and 21 can be inferred.

Two sets of experiments were performed with O_2 partial pressures of 5 and 147 Torr. Figure 11 shows infrared spectra acquired before (A) and after (B) a 3 min irradiation of a mixture of 98 mTorr of $\text{CH}_3\text{CF}_2\text{CH}_3$ and 456 mTorr of F_2 in 700 Torr total pressure of air diluent. Spectrum C shows the result of subtracting spectrum A from B. A sample of the aldehyde $\text{CH}_3\text{CF}_2\text{CHO}$ was not available to us, and so we do not have a reference spectrum of this compound. The bottom panel shows reference spectra of CF_3CHO and COF_2 . On the basis of the similarity of the spectrum of the product (C) with the CF_3CHO spectrum, and the expectation that either $\text{CH}_3\text{CF}_2\text{CHO}$ or COF_2 , or both, will be formed, we conclude that the feature in spectrum C at $1725\text{--}1800 \text{ cm}^{-1}$ is attributable to $\text{CH}_3\text{CF}_2\text{CHO}$. The similarity of the rotational envelope of $\text{CH}_3\text{CF}_2\text{CHO}$ and CF_3CHO and the similar mass of F and CH_3 groups suggest that the rotational structure and intensities in the two molecules are very similar. Assuming that the changes in the dipole moments associated with carbonyl stretching are similar, then the integrated absorption of this feature should be comparable in the two species. Hence, comparing the integrated absorption of the product in the region $1725\text{--}1800 \text{ cm}^{-1}$ with that of the calibrated CF_3CHO reference spectrum gives an estimate of the concentration of $\text{CH}_3\text{CF}_2\text{CHO}$.

Figure 12 shows a plot of formation of $\text{CH}_3\text{CF}_2\text{CHO}$ versus the loss of $\text{CH}_3\text{CF}_2\text{CH}_3$. Small amounts of COF_2 product were also observed. As shown in Figure 12, the molar yield of COF_2 increased with the consumption of $\text{CH}_3\text{CF}_2\text{CH}_3$. Such a trend is indicative of secondary reactions forming COF_2 . The reaction

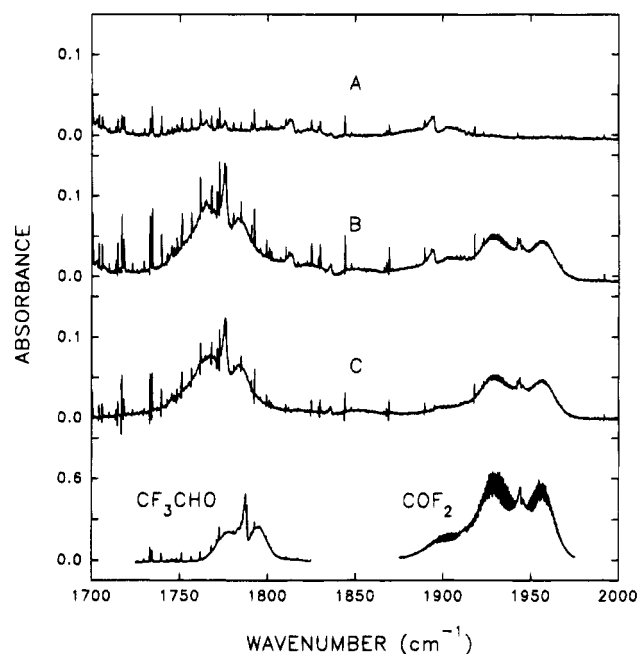


Figure 11. Infrared spectra acquired before (A) and after (B) a 3 min irradiation of a mixture of 98 mTorr of $\text{CH}_3\text{CF}_2\text{CH}_3$ and 456 mTorr of F_2 in 700 Torr of air diluent. Spectrum C = B - A. At the bottom panel shows reference spectra of CF_3CHO and COF_2 .

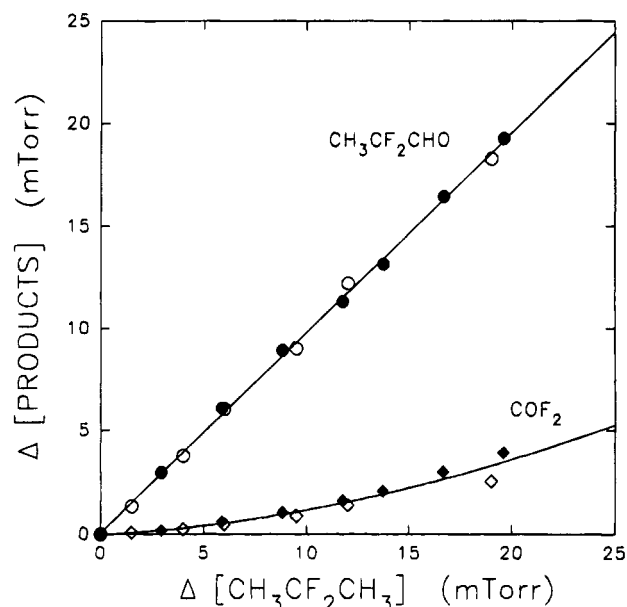


Figure 12. Formation of $\text{CH}_3\text{CF}_2\text{CHO}$ (circles) and COF_2 (diamonds) as a function of the loss of $\text{CH}_3\text{CF}_2\text{CH}_3$ following the irradiation of mixtures of 98–100 mTorr of $\text{CF}_3\text{CH}_2\text{CF}_3$, 0.4–0.5 Torr of F_2 , and either 5 (open symbols) or 147 (filled symbols) Torr of O_2 in 700 Torr total pressure of N_2 diluent. The lines through the $\text{CH}_3\text{CF}_2\text{CHO}$ and COF_2 data are first- and second-order regressions, respectively.

of F atoms with $\text{CH}_3\text{CF}_2\text{CHO}$ is expected to lead to COF_2 formation, although somewhat surprisingly there is no corresponding downward trend discernible in the yield of $\text{CF}_3\text{CF}_2\text{CHO}$. $\text{CH}_3\text{CF}_2\text{CHO}$ and COF_2 together account for 100% of the loss of $\text{CH}_3\text{CF}_2\text{CH}_3$; features attributable to the alcohol $\text{CH}_3\text{CF}_2\text{CH}_2\text{OH}$ were searched for in the O–H stretching region at $3500\text{--}3700 \text{ cm}^{-1}$ with no success.

Linear least squares analysis of the data in Figure 12 gives a $\text{CH}_3\text{CF}_2\text{CHO}$ yield of $97 \pm 5\%$. Quoted errors are 2 standard deviations. There are two possible mechanisms for the formation of $\text{CH}_3\text{CF}_2\text{CHO}$ in the present system: reaction 12b or reaction 12a followed by reaction 20. The rapid reaction of F

atoms with $\text{CH}_3\text{CF}_2\text{CH}_3$ precludes any significant formation of $\text{CH}_3\text{CF}_2\text{CHO}$ via secondary reaction of F atoms with the alcohol $\text{CH}_3\text{CF}_2\text{CH}_2\text{OH}$, which may be formed in reaction 12b. Reaction 12b cannot give a yield of $\text{CH}_3\text{CF}_2\text{CHO}$ greater than 50%. The experimental observation of a yield of $\text{CH}_3\text{CF}_2\text{CHO} = 97 \pm 5\%$ coupled with the low yield of COF_2 shows that under the conditions of the present study reaction with O_2 is essentially the sole fate of $\text{CH}_3\text{CF}_2\text{CH}_2\text{O}$ radicals.

The observation that even with an O_2 partial pressure of 5 Torr the unimolecular decomposition reaction 21 does not compete effectively with reaction 20 serves to define the atmospheric fate of $\text{CH}_3\text{CF}_2\text{CH}_2\text{O}$ radicals. Compared to our 5 Torr O_2 partial pressure experiment, in the atmosphere the O_2 concentration is higher (at least for altitudes below 25 km¹⁷), the temperature is lower, and in general the total pressure is lower. All these factors will further suppress the importance of reaction 21 relative to reaction 20. Reaction 21 is of negligible atmospheric importance.

Implications for Atmospheric Chemistry

Following release into the atmosphere, $\text{CH}_3\text{CF}_2\text{CH}_3$ will react predominantly with hydroxyl radicals. Reaction with OH gives the $\text{CH}_3\text{CF}_2\text{CH}_2$ radical, which within 1 μs will be converted into the corresponding peroxy radical, $\text{CH}_3\text{CF}_2\text{CH}_2\text{O}_2$. We have shown here that $\text{CH}_3\text{CF}_2\text{CH}_2\text{O}_2$ radicals react rapidly with NO and NO_2 . The reaction of $\text{CH}_3\text{CF}_2\text{CH}_2\text{O}_2$ radicals with NO gives NO_2 , and by inference, $\text{CH}_3\text{CF}_2\text{CH}_2\text{O}$ radicals. Reaction of $\text{CH}_3\text{CF}_2\text{CH}_2\text{O}_2$ radicals with NO_2 produces the thermally unstable peroxyxynitrate, $\text{CH}_3\text{CF}_2\text{CH}_2\text{O}_2\text{NO}_2$, which will decompose to regenerate the reactants. In light of the instability of $\text{CH}_3\text{CF}_2\text{CH}_2\text{O}_2\text{NO}_2$ we need not consider the reaction of $\text{CH}_3\text{CF}_2\text{CH}_2\text{O}_2$ with NO_2 further. Using $k_2 = 8.5 \times 10^{-12} \text{ cm}^3 \text{ molecule}^{-1} \text{ s}^{-1}$ together with an estimated background tropospheric NO concentration of $2.5 \times 10^8 \text{ cm}^{-3}$,¹⁹ the lifetime of $\text{CH}_3\text{CF}_2\text{CH}_2\text{O}_2$ radicals with respect to reaction 2 is calculated to be 8 min. Reaction 2 is an important atmospheric loss process for $\text{CH}_3\text{CF}_2\text{CH}_2\text{O}_2$ radicals. We have shown here that the atmospheric fate of the alkoxy radical generated in reaction 2 is reaction with O_2 to give $\text{CH}_3\text{CF}_2\text{CHO}$. Finally, we need to consider the potentially important $\text{CH}_3\text{CF}_2\text{CH}_2\text{O}_2 + \text{HO}_2$ reaction. There are very few measurements of rate constants for the reactions of halogenated peroxy radicals with HO_2 radicals. Reported values for the rate constant for the $\text{CF}_3\text{-CFHO}_2 + \text{HO}_2$ reaction are 4.7×10^{-12} ²⁰ and $4 \times 10^{-12} \text{ cm}^3 \text{ molecule}^{-1} \text{ s}^{-1}$.²¹ Taking an average of these two values and

a global average tropospheric HO_2 concentration of 10^9 cm^{-3} ,¹⁹ the lifetime of $\text{CH}_3\text{CF}_2\text{CH}_2\text{O}_2$ radicals with respect to reaction with HO_2 is calculated to be 4 min. Reaction with HO_2 radicals and with NO are of comparable importance in the atmospheric chemistry of $\text{CH}_3\text{CF}_2\text{CH}_2\text{O}_2$ radicals.

Acknowledgment. O.J.N. would like to thank the Commission of the European Communities for financial support. We thank Roscoe Carter (Ford Motor Co.) for helpful discussions regarding the IR spectrum of $\text{CH}_3\text{CF}_2\text{CHO}$, and Steve Japar (Ford Motor Co.) for a critical reading of the manuscript.

References and Notes

- (1) Wallington, T. J.; Schneider, W. F.; Worsnop, D. G.; Nielsen, O. J.; Debruyne, W.; Shorter, J. A. *Env. Sci. Technol.* **1994**, *28*, 320A.
- (2) Nielsen, O. J.; Gamborg, E.; Sehested, J.; Wallington, T. J.; Hurley, M. D. *J. Phys. Chem.* **1994**, *98*, 9518.
- (3) Sehested, J.; Nielsen, O. J.; Wallington, T. J. *Chem. Phys. Lett.* **1993**, *213*, 457.
- (4) Hansen, K. B.; Wilbrandt, R.; Pagsberg, P. *Rev. Sci. Instrum.* **1979**, *50*, 1532.
- (5) Nielsen, O. J. *Risø-R-480*, 1984.
- (6) Wallington, T. J.; Japar, S. M. *J. Atmos. Chem.* **1989**, *9*, 399.
- (7) Sehested, J.; Sehested, K.; Nielsen, O. J.; Wallington, T. J. *J. Phys. Chem.* **1994**, *98*, 6731.
- (8) Ellermann, T.; Sehested, J.; Nielsen, O. J.; Pagsberg, P.; Wallington, T. J. *Chem. Phys. Lett.* **1994**, *218*, 287.
- (9) Sehested, J.; Ellermann, T.; Bartkiewicz, E.; Nielsen, O. J.; Wallington, T. J.; Hurley, M. D. *Int. J. Chem. Kinet.* **1993**, *25*, 701.
- (10) Wallington, T. J.; Nielsen, O. J. *Chem. Phys. Lett.* **1991**, *187*, 33.
- (11) Sehested, J.; Nielsen, O. J.; Wallington, T. J. *Chem. Phys. Lett.* **1993**, *213*, 457.
- (12) Rasmussen, O. L.; Bjergbakke, E. *Risø-R-395*, 1984.
- (13) Sehested, J. *Int. J. Chem. Kinet.* **1994**, *26*, 1023.
- (14) Wallington, T. J.; Ellerman, T.; Nielsen, O. J.; Sehested, J. *J. Phys. Chem.* **1994**, *98*, 2350.
- (15) Lightfoot, P. D.; Cox, R. A.; Crowley, J. N.; Destriau, M.; Hayman, G. D.; Jenkin, M. E.; Moortgat, G. K.; Zabel, F. *Atmos. Environ.* **1992**, *26A*, 1805.
- (16) Wallington, T. J.; Hurley, M. D. *Chem. Phys. Lett.* **1992**, *189*, 437.
- (17) DeMore, W. B.; Sander, S. P.; Golden, D. M.; Hampson, R. F.; Kurylo, M. J.; Howard, C. J.; Ravishankara, A. R.; Kolb, C. E.; Molina, M. J. *Jet Propulsion Laboratory Publication 92-20*; Pasadena, CA, 1992.
- (18) Wallington, T. J.; Hurley, M. D.; Shi, J.; Maricq, M. M.; Sehested, J.; Nielsen, O. J.; Ellermann, T. *Int. J. Chem. Kinet.* **1993**, *25*, 651.
- (19) Atkinson, R. Scientific Assessment of Stratospheric Ozone. World Meteorological Organization Global Ozone Research and Monitoring Project, Report No. 20; 1989; Vol. 2, p 167.
- (20) Maricq, M. M.; Szenté, J. J.; Hurley, M. D.; Wallington, T. J. *J. Phys. Chem.* **1994**, *98*, 8962.
- (21) Hayman, G. AFEAS Workshop on Atmospheric Degradation of HFCs and HFCS, Boulder, CO, Nov 1993.

JP942529M